not heat up the cloud and destroy the condensate, it will change its phase as a result of frequency shifts by the ac Stark effect. This still allows a nonperturbative measurement of the number of condensed atoms, which is the variable complementary to the phase (so-called quantum nondemolition measurement), and would be the inverse situation compared to related measurements in microwave cavities where the photon number can be determined from the phase shift of Rydberg atoms passing through the cavity (*23*).

## REFERENCES AND NOTES


1. A. Griffin, D. W. Snoke, S. Stringari, Eds., *Bose-Einstein Condensation* (Cambridge Univ. Press, Cambridge, 1995).
2. K. Huang, *Statistical Mechanics* (Wiley, New York, ed. 2, 1987).
3. W. E. Lamb Jr. and A. Nordsieck, *Phys. Rev.* **59**, 677 (1941).
4. P. E. Sokol, in (*1*), pp. 51–85.
5. J. L. Lin and J. P. Wolfe, *Phys. Rev. Lett.* **71**, 1222 (1993).
6. M. H. Anderson, J. R. Ensher, M. R. Matthews, C. E. Wieman, E. A. Cornell, *Science* **269**, 198 (1995).
7. K. B. Davis *et al.*, *Phys. Rev. Lett.* **75**, 3969 (1995).
8. T. J. Greytak, in (*1*), pp. 131–159.
9. W. Petrich, M. H. Anderson, J. R. Ensher, E. A. Cornell, *Phys. Rev. Lett.* **74**, 3352 (1995).
10. K. B. Davis *et al.*, *ibid.*, p. 5202.
11. E. Arimondo, W. D. Phillips, F. Strumia, Eds., *Proceedings of the International School of Physics "Enrico Fermi," Course CXVIII* (North-Holland, Amsterdam, 1992).
12. C. C. Bradley, C. A. Sackett, J. J. Tollett, R. G. Hulet, *Phys. Rev. Lett.* **75**, 1687 (1995).
13. Book of abstracts, *Workshop on Collective Effects in Ultracold Atomic Gases*, Les Houches, France, 1–5 April 1996.
14. E. Hecht, *Optics* (Addison-Wesley, Reading, MA, ed. 2, 1989).
15. M.-O. Mewes *et al.*, *Phys. Rev. Lett.*, in press.
16. D. E. Pritchard, K. Helmerson, A. G. Martin, in *Atomic Physics 11*, S. Haroche, J. C. Gay, G. Grynberg, Eds. (World Scientific, Singapore, 1989), pp. 179–197; W. Ketterle and N. J. van Druten, in *Advances in Atomic, Molecular and Optical Physics*, B. Bederson and H. Walther, Eds. (Academic Press, San Diego, in press), vol. 37.
17. It was a coincidence that the ideal detuning for this work was close to the 1.77 GHz ground-state hyperfine splitting in sodium.
18. S. R. de Groot, G. J. Hooyman, C. A. ten Seldam, *Proc. R. Soc. London Ser. A* **203**, 266 (1950).
19. G. Baym and C. J. Pethick, *Phys. Rev. Lett.* **76**, 6 (1996).
20. L. You, M. Lewenstein, R. J. Glauber, J. Cooper, *Phys. Rev. A* **53**, 329 (1996).
21. J. Javanainen, *Phys. Rev. Lett.* **72**, 2375 (1994).
22. O. Morice, Y. Castin, J. Dalibard, *Phys. Rev. A* **51**, 3896 (1995).
23. M. Brune *et al.*, *Phys. Rev. Lett.* **65**, 976 (1990).


24. We are grateful to D. Pritchard for valuable comments on the manuscript and thankfully acknowledge C. Townsend for assistance in the final stages of the experiment. This work was supported by the Office of Naval Research, NSF, Joint Services Electronics Program, and the Sloan Foundation. M.-O.M. and D.M.K. acknowledge financial support from Studienstiftung des Deutschen Volkes and an NSF Graduate Research Fellowship, respectively, and N.J.v.D., from Nederlandse Organisatie voor Wetenschappelijk Onderzoek (NWO) and Netherlands America Commission for Education Exchange (Fulbright fellowship).

29 May 1996; accepted 11 June 1996


# Homogeneous Linewidths in the Optical Spectrum of a Single Gallium Arsenide Quantum Dot


D. Gammon,* E. S. Snow, B. V. Shanabrook, D. S. Katzer, D. Park



The homogeneous linewidths in the photoluminescence excitation spectrum of a single, naturally formed gallium arsenide (GaAs) quantum dot have been measured with high spatial and spectral resolution. The energies and linewidths of the homogeneous spectrum provide a new perspective on the dephasing dynamics of the exciton in a quantum-confined, solid-state system. The origins of the linewidths are discussed in terms of the dynamics of the exciton in zero dimensions, in particular, in terms of lifetime broadening through the emission or absorption of phonons and photons.


Excitons are the quanta of excitation in semiconductors that are composed of an electron excited across the band gap bound to the hole left behind. Localization of the exciton in all three dimensions changes the density of states from a continuous band structure to one that is "atomic-like" and strongly modifies the optical spectrum. Large variations in the magnitude of localization lead to variations in the energies of the different excitons and consequently to inhomogeneous broadening of the spectral features. However, the rate at which a given exciton is scattered is greatly reduced by localization, which dramatically decreases the homogeneous linewidth (*1*, *2*). This effect was first measured in GaAs-$Al_xGa_{1-x}As$ quantum well structures by Hegarty *et al.* (*3*) and subsequently by many other groups, although only with the rather indirect methods of nonlinear spectroscopy (*1*, *4*) and light scattering (*3*, *5*, *6*) on large inhomogeneous ensembles. We discuss here a direct measurement of the homogeneous linewidth of a single localized exciton.

In narrow quantum wells, localization occurs in one of the dimensions through the quantum-well potential and in the other two dimensions through random variations in the quantum-well width arising from monolayer fluctuations in the position of the interface (schematic in Fig. 1). In some cases, the localized excitons in quantum wells can be treated as a dilute but weakly bound system of "zero-dimensional" (0D) quantum dots (Qdots). Local spectroscopic techniques, such as near-field optical microscopy, can be used to probe an individual Qdot (*7–10*) and to measure its excited states (*9*, *10*). We can measure directly the homogeneous linewidth because, by looking at a single Qdot, all inhomogeneous broadening is removed. This allows us to measure the homogeneous linewidth of a localized exciton along with its excited-state spectrum. We can simultaneously obtain a direct measure of the homogeneous linewidths of the exciton ground and excited states and determine the size of the Qdot potential as parameterized by the energy separations of the quantized states. We compare the measured Qdot homogeneous linewidths with those expected if the 0D exciton dynamics (*2*, *11–13*) are dominat-

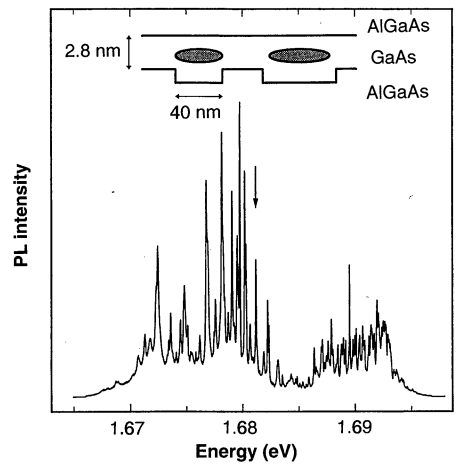


**Fig. 1.** Nonresonant (laser energy, 2.4 eV) PL measured through an aperture 1.5 μm in diameter. The sharp lines arise from the Qdot potentials discussed in the text. The clustering of the sharp lines into two broad features centered at 1.677 and 1.690 eV arises from fluctuations of one monolayer (0.3 nm) in the quantum-well width, whereas the distribution within the broad peaks arises from fluctuations in the lateral sizes of the Qdots. The arrow points to the Qdot line that is discussed in detail here. The inset shows schematically (not to scale) the monolayer fluctuations in the quantum-well interfaces that lead to the localization of the excitons (ovals) into Qdot potentials.


Naval Research Laboratory, Washington, DC 20375, USA.

*To whom correspondence should be addressed. E-mail: gammon@bloch.nrl.navy.mil

ed by emission or absorption of phonons and photons.

We obtained photoluminescence (PL) and PL excitation spectra from a 2.8-nm-thick GaAs quantum well grown by molecular-beam epitaxy with 2-min growth interrupts at each interface. The GaAs quantum well was surrounded by 25-nm-thick $Al_{0.3}Ga_{0.7}As$ barriers and capped with a 50-nm GaAs layer. Similar results were obtained from a 4.2-nm quantum well 30 nm deeper in the sample. With growth interrupts, the interfaces develop large (compared to the exciton Bohr radius of ≈10 nm) monolayer-high islands. The variation in potential arising from the monolayer changes in well width forms the lateral potential that defines the Qdot. Such structures provide a model system for studying quantum dots because the lateral confinement is established in a defect-free manner (*7–10*).

Macroscopic PL measurements on such samples merge the PL peaks from a large number of individual Qdots to form a continuous inhomogeneously broadened peak. If individual Qdots are to be probed, the spatial resolution must be on the micrometer scale or better. We used electron-beam lithography and metal liftoff to open a series of apertures in a 100-nm-thick Al film that was deposited on the surface. The holes, ranging in size from 25 to 0.2 μm, were spaced sufficiently far apart to allow optical probing of a single aperture. The PL was excited and detected through the same hole with either an Ar laser or a Ti:sapphire laser with a power density of ≈10 W $cm^{-2}$. The PL was detected with a Dilor triple spectrometer with a charge-coupled device detector. Linear polarizations along (110) axes were used.

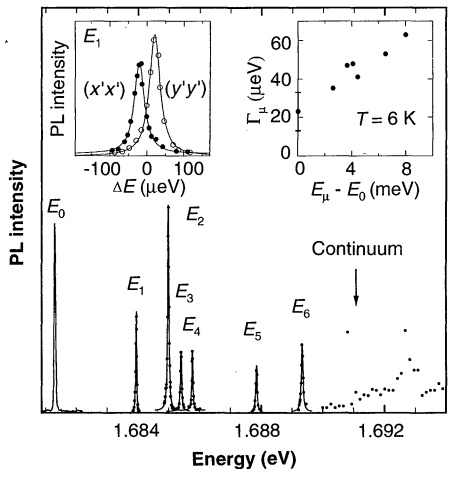


**Fig. 2.** The PL line ($E_0$) shown by the arrow in Fig. 1 and its associated PL excitation spectrum measured with the (*y'y'*) polarization configuration. The arrow denotes approximately the onset of the continuum. Each line is actually a doublet, as shown for the first excited state ($E_1$) in the left inset. The right inset shows the linewidths ($\Gamma_\mu$) (FWHM) as a function of the energy difference between the excited and ground exciton states ($E_\mu - E_0$).

By reducing the effective area of the sample to micrometer dimensions with the metal apertures, we were able to reduce the number of Qdots illuminated so that only a few Qdots luminesced (Fig. 1). The sharp PL lines arise from the ground-state PL of individual Qdots within the aperture. Because they are sufficiently separated in energy, we can tune the laser into resonance with the excited state of a single Qdot such that a single strong PL peak is observed with an energy corresponding to the ground state of that particular dot. As discussed in (*10*), we could map the excited states of a single Qdot by scanning the laser and recording such resonances, and thereby estimate the lateral size of a Qdot. Furthermore, the polarization dependence of the PL and PL excitation spectra reveals an asymmetry in the shape of the Qdot potential (*14*). Here we focus on the spectral linewidths measured by this technique and discuss their origins.

Figure 2 shows the excitation spectrum of the Qdot PL line identified by the arrow in Fig. 1. The spectrum in Fig. 2 is analogous in many ways to the discrete spectrum measured in atoms and molecules. The peaks in the excitation spectrum correspond to the discrete excited states of the lateral potential. The Qdot potential can be modeled as a disk with a relatively small potential offset in the plane of the disk arising from changes in the quantum-well width as a result of the interface fluctuations of one monolayer. For this sample the lateral potential depth is about 11 meV, and for this Qdot the lateral diameter is on the order of 40 nm (*10*). The potential offset in the normal dimension is due to the $Al_{0.3}Ga_{0.7}As$ quantum-well barriers and is much larger (300 meV). For excitation energies greater than the difference between the depth of the lateral potential and the ground-state energies, two-dimensional (2D) excitons are created. The approximate onset of this quasi-2D continuum is shown by the arrow in Fig. 2.

In 2D quantum wells, the exciton line is twofold degenerate. However, because of the elongated Qdot potential, this spin degeneracy is lifted, and the ground-state PL is split into two linearly polarized components (*14–16*). By detecting either one or the other and using parallel polarized exciting and detected light, we measure two separate ladders of excited states in the PL excitation spectrum (that is, doublets for each of the excited states). Both components of the first excited state are shown in the left inset to Fig. 2. In crossed polarizations, (*x'y'*) or (*y'x'*), the signal is much weaker. This strong polarization memory implies that spin-flip scattering is much slower than the rate at which excitons relax to the ground state by emitting acoustic phonons and also slower than the radiative recombination rate from the ground state.

The excitation spectral lines are very narrow and well fit by Lorentzian functions (left inset, Fig. 2). The linewidths [full width at half maximum (FWHM)] are plotted as a function of the energy difference between the excited states and the ground state (right inset, Fig. 2). The linewidths measured in the (*x'x'*) and (*y'y'*) configurations are similar. The resolution of the excitation spectroscopy is that of the laser (7 μeV), and the excited-state linewidths are fully resolved. The resolution of the PL is determined by the spectrometer (30 μeV), and the ground-state linewidth (45 μeV) is partially resolved. A deconvolution of the spectrometer response yields a value of 23 ± 10 μeV for the ground-state linewidth (*17*). We were careful to ensure that heating or other laser-induced effects did not artificially broaden the lines.

The homogeneous linewidths yield the exciton scattering rates (*18*). Let us consider what scattering processes are possible. In both two and three dimensions, the fastest exciton dynamics are governed by elastic scattering, phonon scattering, spin-flip scattering, and radiative recombination (*19*). However, in Qdots the scattering mechanisms should be suppressed. First, the complete quantization of the available energy states prohibits elastic scattering (*2*). Moreover, at low temperature the exciton ground state is not scattered by phonons because phonon emission is forbidden by energy conservation and phonon absorption is unlikely because the first excited state that does not require a spin flip is 2.7 meV higher in energy. We neglect the possibility of spectral diffusion [such as phonon-assisted tunneling (*1–5*)], because, when this Qdot is selectively excited, the PL from other Qdots is at least an order of magnitude weaker. This result implies that energy migration between Qdots is negligible, which is not surprising because of the low density of these Qdots (*14, 20*). Furthermore, the polarization memory observed in the PL excitation spectra implies that the spin-flip rates are much smaller than the radiative recombination rate. Thus, we conclude that radiative broadening is the most likely origin of the linewidth of the ground-state PL at low temperature. The measured ground-state linewidth of the Qdot of 23 μeV implies a radiative rate of $3.5 \times 10^{10}$ $s^{-1}$ (lifetime, 29 ps). This value is in good agreement with the calculation of Bockel-

mann (*12*) for the radiative rate of the exciton in a GaAs Qdot with a comparable excited-state splitting. Furthermore, this measured value for the Qdot linewidth is narrower by a factor of 4 than that expected for the radiative linewidth for a 3-nm quantum well (*11*, *21*, *22*), as expected (*11*).

With increasing temperature $T$, the linewidth of the ground-state PL increases (Fig. 3). Scattering of the exciton into higher energy states increases and is accompanied by the absorption of thermally created acoustic phonons. From perturbation theory, the scattering rate for the $\mu$th exciton state, $\Gamma_\mu(T)$, can be written as

$$\Gamma_\mu(T) = \Gamma_\mu + \sum_{\nu>\mu} \gamma_{\mu\nu}\cdot n(E_{\mu\nu},T) + \sum_{\nu<\mu} \gamma_{\mu\nu}\cdot[n(E_{\mu\nu},T)+1] \quad (1)$$

where $n(E_{\mu\nu},T) = [\exp(E_{\mu\nu}/kT)-1]^{-1}$ is the Bose function that describes the number of acoustic phonons with energies equal to a transition energy ($E_{\mu\nu}$), $k$ is Boltzmann's constant and $\gamma_{\mu\nu} = \gamma_{\nu\mu}$ contains the exciton-phonon matrix element between the $\mu$th and $\nu$th state (schematic in Fig. 3) (*12*). The first term on the right in Eq. 1 comes from those contributions to the scattering rate that do not involve phonons. In the discussion above we have concluded that for the ground state ($\mu = 0$) this term is in large part due to radiative recombination. The second term in Eq. 1 is due to phonon absorption and involves a sum over transitions into higher energy states. It goes to zero with the temperature because $n(E,T = 0) = 0$. The last term is due to phonon emission. It involves a sum over transitions to lower energy states and therefore is zero for the ground state at all temperatures.

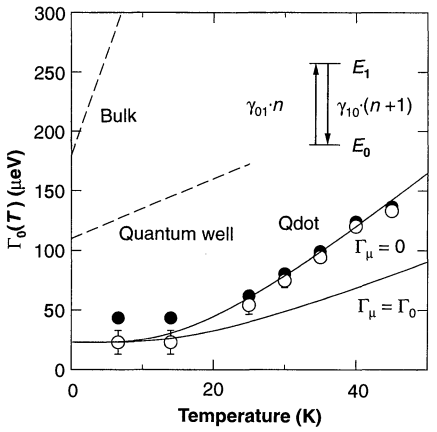


**Fig. 3.** The temperature dependence of the ground-state linewidth before (filled symbols) and after (open symbols) deconvolution of the spectrometer response. The solid curves are from the model calculation discussed in the text. The dashed curves are previously measured homogeneous linewidths from four-wave–mixing measurements on a 12-nm-wide GaAs-AlGaAs quantum well and on a bulk-like 194-nm GaAs layer (*23*). The inset is a schematic of the transitions between Qdot energy levels.

The thermal broadening of the ground state is given by the second term on the right in Eq. 1. In earlier studies (*3*–*6*) of localized excitons in this temperature range, the sum over excited states has been replaced by a single term to obtain a fitted activation energy. If we make this substitution, we obtain an activation energy of 6 meV, which is significantly less than the ≈11 meV into the continuum. This result reflects the importance of the excited discrete states.

A comparison between the thermal broadening of the Qdot exciton line and that measured previously (*23*) with four-wave-mixing on quasi-2D quantum well and quasi-3D bulk GaAs samples is shown in Fig. 3. In contrast to the activated Qdot behavior, 2D and 3D excitons have a continuum of excited states that leads to a linear temperature dependence for the thermal broadening (*24*). Moreover, the zero-temperature homogeneous linewidths of the quantum well and the bulk samples are considerably greater than that of the Qdot, as expected from the discussion given earlier.

We now discuss the origin of the excited-state linewidths. In addition to radiative recombination, the excited states can also decay by the emission of an acoustic phonon even at the lowest temperature. We observe a systematic increase in linewidth with increasing energy of the excited state (right inset, Fig. 2). Because the radiative contribution to the linewidth of the excited states is expected to be less than the 23 μeV measured for the ground state (*12*), this systematic increase in linewidth likely arises from an increased phonon emission rate. This increase is not surprising because (i) the high-energy excitons can decay into a larger number of final states, (ii) the requirement to conserve energy in an $E_{\nu 0}$ scattering event is satisfied by a larger phonon density of states for large $\nu$, and (iii) for weak confinement the exciton-phonon matrix element increases with the wave vector of the phonon (*12*). We conclude that a significant fraction of the excited-state linewidths is due to phonon emission. This conclusion also explains our inability to observe PL from the excited states. For the first excited state, the linewidth of 35 μeV yields a scattering rate of $5.3\times10^{10}$ s$^{-1}$ (lifetime, 19 ps). This value is in good agreement with the calculated phonon emission rate from an excited state of a GaAs Qdot with a comparable transition energy (*12*). This result indicates the absence of a significant phonon bottleneck (*12*, *13*), which is in agreement with the calculation of Bockelmann (*12*) for Qdots with lateral confinement energies in this range.

Measurements of the excited-state linewidths allow us to go somewhat further in comparing Eq. 1 to the measured thermal broadening of the exciton ground state. To calculate $\Gamma_0(T)$ using Eq. 1, we need the energy separations ($E_{0\nu}$) and the $\gamma_{0\nu}$. The $E_{0\nu}$ can be taken directly from the spectrum, and as we show now, we can estimate the $\gamma_{\mu\nu}$ from the low-temperature, excited-state linewidths. In particular, the first excited-state linewidth is given by $\Gamma_1 + \gamma_{01}$ because $n(E,T = 0) = 0$. We estimate $\gamma_{01}$ from the measured linewidth by taking either $\Gamma_1 = 0$ (no radiative broadening for the excited state) or $\Gamma_1 = \Gamma_0$ (the excited state and ground state have equal radiative linewidths). The value of $\Gamma_1$ should be somewhere in between (*12*). This calculation can be done for each of the excited state linewidths, although for the higher excited states we also neglect contributions from transitions into intermediate states. If we carry out this calculation using the first six excited states, we obtain the two solid curves shown in Fig. 3. In both cases, we have neglected the contribution of the continuum, which will increase the calculated values. From the rough agreement between the calculation and the data, we conclude that the magnitude of the thermal broadening of the ground-state linewidth is consistent with the excited-state spectrum and with our assertion that the excited-state linewidths are in large part due to phonon broadening.

We have measured an order-of-magnitude reduction in total linewidth compared to those measured in the best quantum-well samples (*25*). This result occurs through the complete removal of inhomogeneous broadening in the measurement of a single Qdot combined with the reduction in homogeneous broadening as the scattering slows down in going to the fully quantized, 0D Qdot.

## REFERENCES AND NOTES


1. J. Hegarty and M. D. Sturge, *J. Opt. Soc. Am. B* **2**, 1143 (1985).
2. T. Takagahara, *J. Lumin.* **44**, 347 (1989).
3. J. Hegarty, M. D. Sturge, C. Weisbuch, A. C. Gossard, W. Wiegmann, *Phys. Rev. Lett.* **49**, 930 (1982); J. Hegarty, L. Goldner, M. D. Sturge, *Phys. Rev. B* **30**, 7346 (1984).
4. H. Wang, M. Jiang, D. G. Steel, *Phys. Rev. Lett.* **65**, 1255 (1990).
5. J. E. Zucker, A. Pinczuk, D. S. Chemla, A. C. Gossard, *Phys. Rev. B* **35**, 2892 (1987).
6. A. J. Shields, *et al.*, *ibid.*, **48**, 17338 (1993).
7. H. F. Hess, E. Betzig, T. D. Harris, L. N. Pfeiffer, K. W. West, *Science* **264**, 1740 (1994).
8. Z. Zrenner *et al.*, *Phys. Rev. Lett.* **72**, 3382 (1994).
9. K. Brunner, G. Abstreiter, G. Bohm, G. Trankle, G. Weimann, *Appl. Phys. Lett.* **64**, 3320 (1994); *Phys. Rev. Lett.* **73**, 1138 (1994).
10. D. Gammon, E. S. Snow, D. S. Katzer, *Appl. Phys. Lett.* **67**, 2391 (1995).

11. D. S. Citrin, *Phys. Rev. B* **47**, 3832 (1993).
12. U. Bockelmann, *ibid.* **48**, 17637 (1993).
13. H. Benisty, *ibid.* **51**, 13281 (1995).
14. D. Gammon, E. S. Snow, B. V. Shanabrook, D. S. Katzer, D. Park, *Phys. Rev. Lett.* **76**, 3005 (1996).
15. H. W. van Kesteren, E. C. Cosman, W. A. J. A. van der Poel, C. T. Foxon, *Phys. Rev. B* **41**, 5283 (1990).
16. E. Blackwood, M. J. Snelling, R. T. Harley, S. R. Andrews, C. T. B. Foxon, *ibid.* **50**, 14246 (1994).
17. To obtain this result, we used the measured spectrometer response function and assumed that the excitonic ground-state line shape is Lorentzian, as observed for the excited states (left inset, Fig. 2).
18. The homogeneous linewidth is determined by the total dephasing rate which in general is given by the exciton lifetime term $\tau^{-1}$ discussed in the text plus a pure dephasing term [see, for example, M. D. Webb, S. T. Cundiff, D. G. Steel, *Phys. Rev. B* **43**, 12658 (1991)]. For resonant excitation of a single Qdot at low temperature and power density, the pure dephasing rate should be small, and we ignore it in our discussion. We take $\tau^{-1} = \Gamma$ (FWHM)/$\hbar$, where $\hbar$ is Planck's constant divided by $2\pi$.
19. A. Vinattieri *et al.*, *Phys. Rev. B* **50**, 10868 (1994).
20. In this sense our localized exciton system is qualitatively different from that examined in the earlier linewidth studies (*1–5*). This difference arises from the use of growth interrupts at the interfaces in our samples, which completely changes the spectral and spatial distribution of the localized states [see, for example, D. Gammon *et al.*, *Appl. Phys. Lett.* **57**, 2710 (1990)].
21. L. C. Andreani, F. Tassone, F. Bassani, *Solid State Commun.* **77**, 641 (1991); L. C. Andreani in *Confined Electrons and Photons*, E. Burstein and C. Weisbuch, Eds. (Plenum, New York, 1995), p. 57.
22. B. Deveaud *et al.*, *Phys. Rev. Lett.* **67**, 2355 (1991).
23. J. Kuhl, A. Honold, L. Schultheis, C. W. Tu, *Festkoerperprobleme* **29**, 157 (1989).
24. Published values of $\gamma$ for quantum wells vary from 2.5 $\mu$eVK$^{-1}$ for a 12-nm quantum well, as shown in Fig. 3, to 9 $\mu$eVK$^{-1}$ for a 28-nm quantum well (*23*).
25. V. Srinivas, Y. J. Chen, C. E. C. Wood, *Phys. Rev. B* **46**, 10193 (1992); D. Gammon, S. Rudin, T. L. Reinecke, D. S. Katzer, C. S. Kyona, *ibid.* **51**, 16785 (1995).
26. This research was funded in part by the office of Naval Research.

4 March 1996; accepted 15 May 1996

# Two Calorimetrically Distinct States of Liquid Water Below 150 Kelvin

G. P. Johari,* Andreas Hallbrucker, Erwin Mayer

**Vapor-deposited amorphous solid and hyperquenched glassy water were found to irreversibly transform, on compression at 77 kelvin, to a high-density amorphous solid. On heating at atmospheric pressure, this solid became viscous water (water B), with a reversible glass-liquid transition onset at 129 ± 2 kelvin. A different form of viscous water (water A) was formed by heating the uncompressed vapor-deposited amorphous solid and hyperquenched liquid water. On thermal cycling up to 148 kelvin, water B remained kinetically and thermodynamically distinct from water A. The occurrence of these two states, which do not interconvert, helps explain both the configurational relaxation of water and stress-induced amorphization.**

Amorphous solid water can be prepared by vapor deposition on a metal substrate kept at 100 K or below (*1*). In 1980, it was first shown that liquid water, when cooled at rates of $\approx 10^6$ to $\approx 10^7$ K s$^{-1}$, also produced an amorphous solid known as hyperquenched glassy water (*2*). Four years later, it was observed that uniaxial compression of hexagonal ice to 10 kbar at 77 K produced a new amorphous solid (*3*) called high-density amorph (HDA). Its density of 1.31 g cm$^{-3}$ at 77 K and 10 kbar decreases to 1.17 g cm$^{-3}$ on decompression to 1 bar, and its x-ray and neutron diffraction patterns are quite distinct from those of the amorphous forms obtained from vapor deposition or by hyperquenching water, all at 1 bar (*3–6*). Cubic ice is also found to collapse in a similar manner to HDA (*7, 8*) but not ice clathrate (*9*). On heating to 125 K at 1 bar, HDA (1.17 g cm$^{-3}$) transforms irreversibly and exothermally to a low-density amorph (LDA). This in turn undergoes a glass-to-liquid transition with an onset temperature of 129 ± 2 K (referred to as its $T_g$) on heating at 30 K min$^{-1}$ (*8, 10*) or of 124 K on heating at 0.17 K min$^{-1}$ (*11*). Upon further heating to far above its $T_g$, the now metastable state of viscous liquid water crystallizes to cubic ice extremely rapidly at ≈150 K.

In our continuing experimental studies of the thermodynamics of the solid forms of amorphous water, we have discovered that vapor-deposited amorphous solid water and hyperquenched glassy water, whose $T_g$ values are both 136 ± 1 K for heating at 30 K min$^{-1}$ (*12, 13*), collapse also under a uniaxial pressure to produce a high-density amorphous solid at 77 K. On heating at 1 bar, this solid transforms exothermally and irreversibly to a low-density amorphous solid that, on further heating, undergoes a glass-to-liquid transition at 129 ± 2 K for heating at 30 K min$^{-1}$. This $T_g$ is the same as that of LDA obtained by uniaxial compression of hexagonal and cubic ices at 77 K (*8, 10*).

Thus, we report here two effects: first, under a uniaxial pressure at 77 K, the amorphous solids—namely, the vapor-deposited amorphous solid water (ASW), the hyperquenched glassy water (HGW), and the crystalline solids (hexagonal and cubic ices)—all collapse to produce HDA. On heating to 125 K at 1 bar, this amorph transforms irreversibly to LDA with $T_g$ = 129 K. Second, this LDA is calorimetrically distinct from ASW and HGW (*12, 13*), although the densities of the three are similar.

Further experiments show that there are two distinct forms of viscous water: water A, which is obtained by heating uncompressed ASW and HGW to above $T_g$ = 136 K and up to 148 K, and water B, which is obtained by heating, at 1 bar, the product of uniaxially compressed ASW, HGW, and hexagonal and cubic ices to 148 K, a temperature above the $T_g$ (129 K) of the amorphous solids. This has implications for our understanding of the water's state in the extraterrestrial bodies where high pressures exist (*14*); here, we consider its implications only for our understanding of irreversible phase transformations under pressure and of configurational relaxations in liquid water.

Vapor-deposited amorphous water (ASW) was prepared by admitting water vapors from a water reservoir held at 298 K through a fine metering valve and a tube of 13 mm inner diameter into a high vacuum system, where the vapors condensed on a demountable Cu substrate (50 mm diameter) precooled to 77 K (*12, 15*). In control experiments of our ASW deposits by x-ray diffraction, no sharp peaks (indicating crystalline ice) were observed (*12*). Because our x-ray technique is sensitive to a crystallinity of >2%, we infer that our ASW was at least 98% amorphous. It was then heated in a vacuum to ≈115 K for reduction of its surface area and closure of micropores, before its exposure to $N_2$. ASW treated this way is called "sintered." A similar treatment has been used in the glass-to-liquid transition of ASW (*12*).

Glassy water (HGW) was prepared by hyperquenching—that is, by acceleration of droplets of water (≈3 μm diameter) from an aerosol by supersonic flow and then by their deposition on a Cu plate held inside a high-vacuum cryostat at 77 K (*13, 16*). One hour of deposition produced a 2- to 3-mm-thick opaque layer of glassy solid water with a porcelainlike appearance and texture. According to x-ray diffractograms, it contained

G. P. Johari, Department of Materials Science and Engineering, McMaster University, Hamilton, Ontario L8S 4L7, Canada.
A. Hallbrucker and E. Mayer, Institut für Allgemeine, Anorganische und Theoretische Chemie, Universität Innsbruck, A-6020 Innsbruck, Austria.
*To whom correspondence should be addressed.